

Influence of Plasma-Enhanced Chemical Vapor Deposition Poly-Si Layer Thickness on the Wrap-Around and the Quantum Efficiency of Bifacial *n*-TOPCon (Tunnel Oxide Passivated Contact) Solar Cells

Benjamin Grübel,* Henning Nagel, Bernd Steinhauser, Frank Feldmann, Sven Kluska, and Martin Hermle

In typical industrial processing of tunnel oxide passivated contact (TOPCon) solar cells, poly-Si is deposited on the entire back of the cells. During the deposition process, a wrap-around of poly-Si onto the edges and the front side of the cells is virtually unavoidable if chemical vapor deposition processes are used. Plasma-enhanced chemical vapor deposition (PECVD) is used to investigate very thin poly-Si films and their effect on wrap-around on bifacial TOPCon solar cells fabricated without wrap-around etching. As a result, reduction of the poly-Si thickness down to 30 nm significantly increases the shunt resistance, reduces the reverse bias current, and thus reduces the risk of hot spots as measured by IR imaging and microcharacterization by secondary electron microscopy. Electroplated metallization proves to be a suitable candidate for contacting such thin TOPCon layers, being less sensitive than screen-printed metallization.

1. Introduction

Conventional silicon solar cell concepts such as passivated emitter and rear cells (PERC) are limited by, among others, excess-carrier recombination at the metal–semiconductor interfaces of the front and rear side metallization to the semiconductor.^[1] Introducing a passivating layer in-between that interface such as a tunnel oxide passivated contact (TOPCon) consisting of

an ultrathin SiO_x combined with a highly doped poly-Si layer allows us to significantly reduce contact recombination losses.^[2,3] This way recent achievements of Richter et al. led to a certified record efficiency of 26.0% for a both-side-contacted TOPCon solar cell.^[4]

Industrial upscaling of process steps includes the development of poly-Si film deposition. Currently, the widely used industrial method is low-pressure chemical vapor deposition (LPCVD). It enables in situ formation of the tunnel oxide and allows a conformal deposition of an intrinsic or in situ doped poly-Si layer. An inherent disadvantage of the process is a severe wrap-around even in the case of back-to-back loading, which has to be removed in an additional process step.^[5–7]


Plasma-enhanced chemical vapor deposition (PECVD) is considered a more single-sided deposition technique, although minimal wrap-around can still occur.

Metal contacting of TOPCon layers represents the main challenge in transferring this solar cell concept into an industrially scaled process. To guarantee the full functionality of the TOPCon layer, the metallization process should not damage this layer.^[8] It has been shown by different research groups that TOPCon solar cells with poly-Si thicknesses below 100 nm featuring screen-printed Ag contacts reveal increased contact recombination.^[8–11] However, thinner poly-Si layers are desirable to reduce the deposition time, thereby reducing cost of ownership,^[12,13] free-carrier absorption (FCA) in the highly doped polySi layer^[14] as well as improving the bifaciality factor.^[15] In addition, thinner layers could reduce the etch back time.^[7] Laser ablation and plating of Ni/Cu/Ag contacts was found to be a candidate to allow for metallizing of TOPCon solar cells with thinner poly-Si layers without inducing increased excess carrier recombination.^[9,16]

In this study, the impact of the reduction of the poly-Si layer thickness on the wrap-around during PECVD and the metallization of these TOPCon layers are investigated. The shunt resistance R_{sh} and the current I_{rev} under reverse bias voltage (−12 V) were investigated as a measure of the influence of the wrap-around. Reverse-biased IR imaging^[17–19] for hot spot prediction and microcharacterization by scanning electron

B. Grübel, Dr. H. Nagel, Dr. B. Steinhauser, Dr. S. Kluska, Dr. M. Hermle
Division Photovoltaics
Department Advanced Development for High Efficiency Silicon Solar Cells
Fraunhofer Institute for Solar Energy Systems ISE
Heidenhofstraße 2, 79110 Freiburg im Breisgau, Germany
E-mail: benjamin.gruebel@ise.fraunhofer.de

Dr. F. Feldmann
Solarlab Aiko Europe GmbH
Berliner Allee 29, 79110 Freiburg im Breisgau, Germany

 The ORCID identification number(s) for the author(s) of this article can be found under <https://doi.org/10.1002/pssa.202100156>.

© 2021 The Authors. physica status solidi (a) applications and materials science published by Wiley-VCH GmbH. This is an open access article under the terms of the Creative Commons Attribution License, which permits use, distribution and reproduction in any medium, provided the original work is properly cited.

DOI: 10.1002/pssa.202100156

microscopy (SEM) were used to visualize the poly-Si wrap-around. The effect of reducing the poly-Si layer thickness down to 30 nm on the performance of solar cells was characterized for both electroplated and screen-printed metallization of the TOPCon rear side.

2. Experimental Section

2.1. Sample Preparation

Bifacial TOPCon solar cells were manufactured from $156.75 \times 156.75 \text{ mm}^2$ large n-type Cz-silicon wafers featuring a resistivity of $1 \Omega \text{ cm}$. The exact processing of the solar cells is discussed in detail in the publication of Arya et al.^[16] The schematic cross-sectional layout is shown in Figure 1. The produced TOPCon solar cells feature a thermal SiO_x layer prepared in a tube furnace and a phosphorus-doped amorphous silicon (a-Si) layer deposited in a Centrotherm c.PLASMA tube PECVD with horizontal carrier. The a-Si was transformed to poly-Si by annealing at 900°C for 10 min under a nitrogen atmosphere. The samples were subjected to an O_3/HF solution to remove the poly-Si wrap-around, reducing the poly-Si thickness by about 10 nm. The variation of the poly-Si thickness resulted in thicknesses of 30, 50, 70, and 90 nm, respectively. The poly-Si on the rear side was coated with a SiN_x , whereas the front side features a p-type boron emitter passivated by an $\text{AlO}_x/\text{SiN}_x$ stack. The solar cells were screen printed with a Ag grid on the rear side and a AgAl grid on the front side and fired at a set peak temperature of 820°C , corresponding to an actual wafer temperature of $\approx 720^\circ\text{C}$. In addition, TOPCon solar cells featuring screen-printed contacts on the front side and plated contacts on the rear side were also manufactured for all poly-Si thicknesses.

2.2. Characterization Methods

The finished solar cells were subjected to *IV* measurements (cetusPV-Celltest3/halm), quantum efficiency and reflectance measurements with a step size of 10 nm (pv-tools LOANA) as well as microcharacterization by SEM (Auriga/Zeiss).

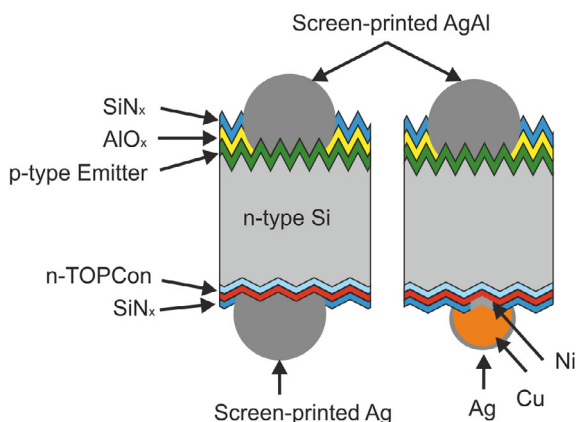


Figure 1. Schematic drawing of the cross-section of both TOPCon solar cell designs with screen-printed contacts on the front side and screen-printed or plated contacts on the rear side, respectively.

The *IV* measurement routine also included fast, reliable, yet quantitative inline hot-spot detection using reverse-biased IR imaging allowing the resolving of smallest temperature changes. Because of the high local power density of hot spots, an approach proposed by Ramspeck et al. was used in this work where an IR image after a very short time (few tens of milliseconds) under reverse voltage of -12 V was taken and subtracted with an IR reference image taken before applying the voltage displaying the temperature change during biasing.^[17]

The microcharacterization to visualize the poly-Si wrap-around in cross-section was performed by use of a scanning electron microscope. This characterization method remains challenging, as the poly-Si layer features the same n-type doping as the bulk material even though different doping levels are present. The thermal oxide between the poly-Si and the bulk is only 1–2 nm thick and is therefore below the resolution limit of the scanning electron microscope. The approach selected here was to mechanically break the solar cell prior to introducing into the scanning electron microscope without further sample preparation. The poly-Si layer could be distinguished from crystalline silicon bulk material due to the columnar shape structure of the poly Si.^[20]

3. Results and Discussion

3.1. Reverse *IV* Characteristic and Thermography

In Figure 2 the shunt resistance R_{sh} and the reverse bias current I_{rev} at -12 V of the solar cells are displayed depending on the poly-Si layer thickness. As plated and screen-printed solar cells revealed the same trend the results are merged in Figure 2. For a poly-Si thickness of 90 nm, I_{rev} reaches values over 10 A and R_{sh} of around $10 \text{ k}\Omega \text{ cm}^2$. Both parameters improve for decreasing poly-Si thicknesses to mean values between 2 and 4 A and above $100 \text{ k}\Omega \text{ cm}^2$ for a poly-Si thickness of 30 nm.

The reverse current and the shunt resistance usually refer to the presence of shunts that bear the risk of hot-spot generation in

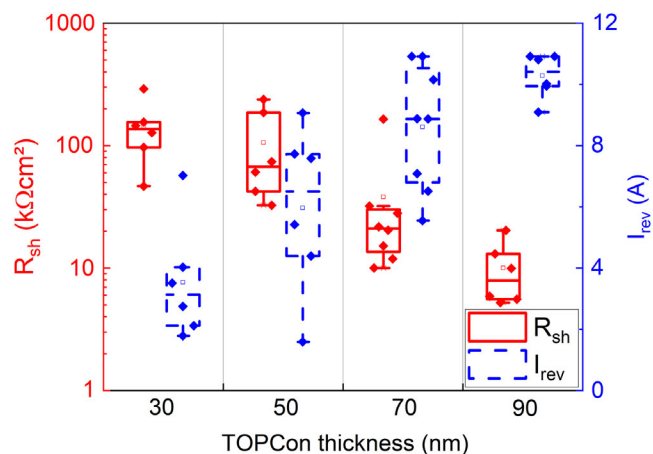


Figure 2. Reverse bias current I_{rev} at -12 V and shunt resistance R_{sh} as a function of poly-Si thicknesses. The screen-printed and plated results are grouped in the same boxes as the trend remained similar independent of the metallization type.

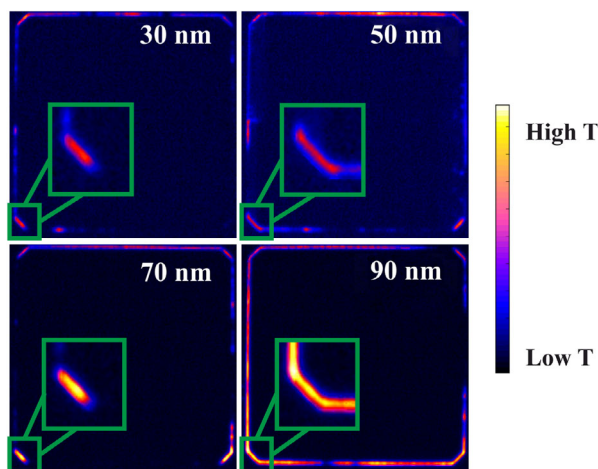


Figure 3. Thermography images taken under reverse voltage (-12 V) of TOPCon solar cells featuring poly-Si layer thicknesses of 30, 50, 70, and 90 nm, respectively.

PV modules manufactured with these cells. This trend decreases with thinner poly-Si layers. **Figure 3** shows thermography images taken under reverse bias voltage of -12 V of solar cells for all poly-Si thicknesses (30–90 nm). For the sample with 90 nm poly-Si almost the whole edge of the solar cell reveals a significant temperature increase. With decreasing poly-Si thickness, the edge proportion and the brightness of increased temperature decrease as well, reducing the risk and severity of hot spots. For the sample with a 30 nm thick poly-Si layer, a smaller share of the edge is thermally visible, whereas a larger share remains thermally inactive.

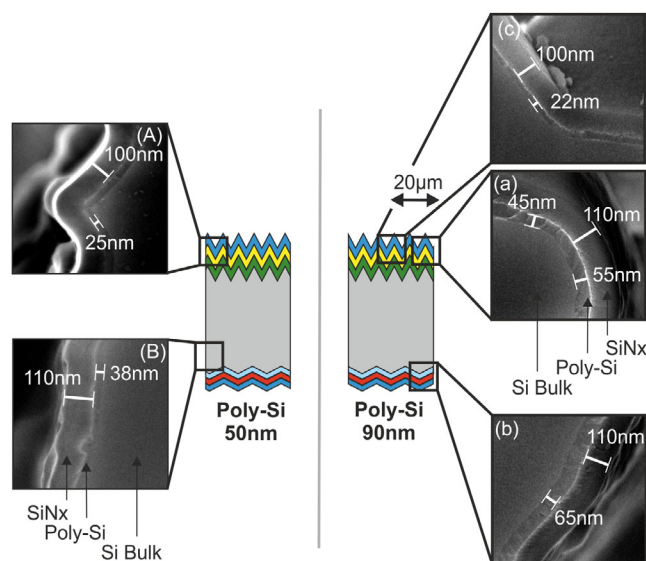


Figure 4. Cross-section images of a TOPCon solar cell with a poly-Si layer thickness of 50 nm (left) and 90 nm (right). For the 50 nm thickness the images were taken at the transition of the front side to the a) edge and on the b) edge close to the rear side. For the 90 nm thickness images on the front side about $20\text{ }\mu\text{m}$ far from the edge (c), at the transition of the front side to the edge (a), and on the transition of the edge to the rear side (b).

3.2. Microcharacterization

Figure 4 shows cross-section SEM images of two TOPCon solar cells shown in **Figure 3** at several positions for 50 nm (A–B) and 90 nm (a–c). The SEM characterization was performed at thermally active positions according to the thermography images as indicated by the green box in **Figure 3**. On both samples, images were taken at the transition of the front side (A, a) and on the edge close to the rear side (B, b). For the sample with a poly-Si thickness of 90 nm, an additional image was taken on the front side $20\text{ }\mu\text{m}$ from the edge. All cross-section images reveal the presence of two layers onto the Si bulk material. The outer layer represents the SiN_x , whereas the intermediate layer represents the TOPCon layer. The sample with a poly-Si layer thickness of 90 nm reveals a poly-Si thickness of 65 nm at position (b), whereas at position (a) a thickness 45–55 nm is measured. On the front side, at position (c) $20\text{ }\mu\text{m}$ from the edge, a poly-Si layer is still measurable with a thickness above 20 nm. Characterization even further away from the edge to identify the wrap-around extent became challenging as the poly-Si layer reaches the limitation of resolution of the used SEM ($<20\text{ nm}$). The sample with a poly-Si thickness of 50 nm (left) at position (B) reveals a poly-Si layer with a thickness of 38 nm. Toward the front side the poly-Si thickness decreases down to a thickness of 25 nm. On the front side itself the poly-Si layer could no longer be identified anymore within range of $20\text{ }\mu\text{m}$ from the edge. The comparison of both samples shows a decrease of the thickness of the poly-Si wrap-around for a lower poly-Si thickness.

3.3. Quantum Efficiency Analysis

In **Figure 5** the internal quantum efficiency (IQE) and reflectance measurements for plated and screen-printed solar cells are shown as a function of the poly-Si thickness in a wavelength range of 800–1200 nm. At a wavelength of 800 nm the IQE

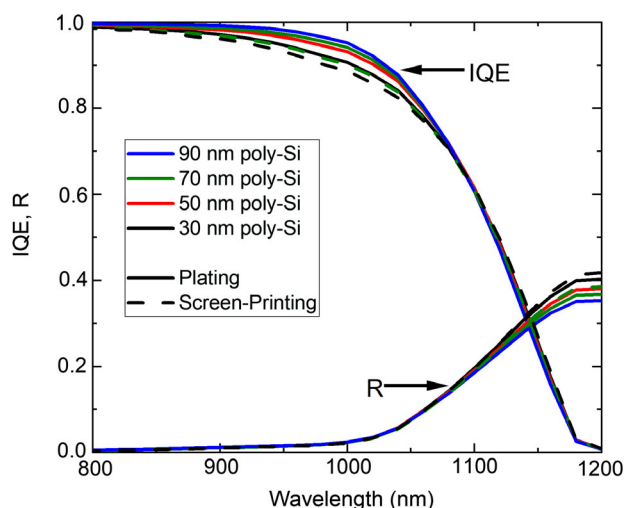


Figure 5. IQE and reflectance curves for selected poly-Si thicknesses. For plating all thicknesses (30, 50, 70, 90 nm) are shown, whereas for screen printing only the results for 30 and 70 nm poly-Si thickness are shown.

Table 1. Average J_{sc} loss compared to the cell with 90 nm poly-si and plated contacts as reference value in the wavelength regime 900–1200 nm ($\Delta J_{sc, 900-1200}$) calculated from the referring external quantum efficiency (EQE) curves from Figure 5 according to the poly-si thickness and the metallization.

Poly-Si thickness [nm]	Metallization on TOPCon	$\Delta J_{sc, 900-1200}$ [mA cm ⁻²]
30	Screen printing	0.41
30	Plating	0.30
50	Plating	0.12
70	Screen printing	0.32
70	Plating	0.11
90	Plating	0 (Reference)

curves start to deviate from each other until they merge again at around 1100 nm. For both metallization approaches, the same trend is visible, that with decreasing poly-Si thickness the IQE is lowered in the mentioned wavelength regime. The samples with a poly-Si thickness of 90 nm and plating metallization reveal the highest IQE curve. The screen-printed sample with a poly-Si thickness of 30 nm features the lowest IQE curve. The IQE curve of the screen-printed sample at a poly-Si thickness of 70 nm is nearly identical to the IQE curve of the plated sample with 30 nm poly-Si thickness. The short circuit current density (J_{sc}) was calculated from the referring external quantum efficiency (EQE) curves from Figure 5 in the wavelength regime 900–1200 nm according to the poly-Si thickness and metallization. In Table 1 the average J_{sc} loss compared to the cell with 90 nm poly-Si and plated contacts as reference value is shown. The observed decrease in the IQE and J_{sc} for thinner poly-Si layers is due to an increase in contact recombination.^[21] The results of increased recombination are in accordance with observations by Arya et al. showing an increase of the contact recombination and that poly-Si layers below 100 nm remain less sensitive to laser ablation than to screen-printing metallization.^[16] Further, the analysis of the IV results of the solar cells presented by Arya et al. reveal a decrease in V_{oc} and J_{sc} for both metallizations whereby the plated cells feature a higher level.^[16] The expected reduction of the FCA can be seen in the increase of the escape reflection for thinner poly-Si layers between 1100 and 1200 nm. According to Feldmann et al. 0.2 mA cm⁻² gain in J_{sc} is expected by reducing the poly-Si thickness from 90 to 30 nm.^[14] However, this reduced FCA cannot be seen in the QE curves. Presumably this gain in J_{sc} is compensated for by the increased contact recombination for thinner poly-Si layers.

4. Conclusion

Single-side TOPCon layer deposition via PECVD leads to a wrap-around of the poly-Si layer onto the front side. This parasitic current path is potentially shunting the solar cells, leading to a lowered shunt resistance. By combining the quantum efficiency results with thermography and microcharacterization with SEM, the poly-Si wrap-around was identified as the reason for the hot-spot generation. Reducing the deposited poly-Si thickness from 90 to 30 nm, the impact of the wrap-around can be diminished,

which improves R_{sh} and I_{rev} . Apart from a shorter deposition time, this approach would also decrease the FCA and increase the bifaciality factor of the solar cells. However, even for a poly-Si layer 30 nm the wrap-around is not fully removed as indicated by elevated I_{rev} and SEM characterization. The IQE of screen-printed TOPCon solar cells was affected by increased contact recombination for thinner poly-Si thicknesses, whereas laser ablation and plating on thin poly-Si layers between 50 and 90 nm was revealed to be less sensitive, thereby allowing higher currents.

Acknowledgements

This work was funded by the German Federal Ministry for Economic Affairs and Energy within the research project “Genesis” (contract no. 0324274C) and “TOPCon Cluster” (contract no. 03EE1065C). The authors want to thank the colleagues at Fraunhofer ISE for their support in preparation and processing of the solar cells.

Open access funding enabled and organized by Projekt DEAL.

Conflict of Interest

The authors declare no conflict of interest.

Data Availability Statement

The data that support the findings of this study are available from the corresponding author upon reasonable request.

Keywords

metallization, passivated contacts, plasma-enhanced chemical vapor deposition, tunnel oxide passivated contacts

Received: April 22, 2021

Revised: May 25, 2021

Published online:

- [1] Y. Zhang, L. Wang, D. Chen, M. Kim, B. Hallam, *J. Phys. D: Appl. Phys.* **2021** *54*, 214003.
- [2] F. Feldmann, M. Bivour, C. Reichel, M. Hermle, S. W. Glunz, *Solar Energy Materials and Solar Cells*. **2014** *120*, 270.
- [3] F. Feldmann, M. Bivour, C. Reichel, M. Hermle, S. W. Glunz, *28th European Photovoltaic Solar Energy Conf.*, <https://www.ise.fraunhofer.de/content/dam/ise/de/documents/publications/conference-paper/28-eupvsec-2013/Feldmann.pdf> (accessed: March 2021).
- [4] A. Richter, R. Müller, J. Benick, F. Feldmann, B. Steinhauser, C. Reichel, A. Fell, M. Bivour, M. Hermle, S. W. Glunz, *Nat Energy*, **2021**, *6*, 429.
- [5] F. Feldmann, T. Fellmeth, B. Steinhauser, H. Nagel, D. Ourinson, S. Mack, E. Lohmüller, J. Polzin, J. Benick, A. Richter, A. Moldovan, M. Bivour, F. Clement, J. Rentsch, M. Hermle, S. W. Glunz, *35th European Photovoltaic Solar Energy Conf.* (Eds: P. Verlinden, R. Kenny, P. Helm), WIP, Munich, Germany **2018**, p. 1.
- [6] M. K. Stodolny, M. Lenes, Y. Wu, G. Janssen, I. G. Romijn, J. Luchies, L. J. Geerligs, *Sol. Energy Mater. Sol. Cells* **2016**, *158*, 24.
- [7] Q. Wang, W. Wu, D. Chen, L. Yuan, S. Yang, Y. Sun, S. Yang, Q. Zhang, Y. Cao, H. Qu, N. Yuan, J. Ding, *Sol. Energy* **2020**, *211*, 324.

- [8] H. E. Çiftçinar, M. K. Stodolny, Y. Wu, G. J. Janssen, J. Löffler, J. Schmitz, M. Lenes, J.-M. Luchies, L. J. Geerligs, *Energy Proc.* **2017**, 124, 851.
- [9] B. Steinhauser, B. Grübel, S. Nold, V. Arya, C. Schmiga, S. Kluska, A. A. Brand, F. Feldmann, N. Bay, N. Bay, X. Gay, M. Passig, M. Glatthaar, in *37th European Photovoltaic Solar Energy Conf.* (Eds: N. Pearsall, R. Kenny, P. Helm), WIP, Munich, Germany **2020**, p. 1.
- [10] P. Padhamnath, A. Khanna, N. Nandakumar, N. Nampalli, V. Shanmugam, A. G. Aberle, S. Dutttagupta, *Sol. Energy Mater. Sol. Cells* **2020**, 207, 110358.
- [11] P. Padhamnath, J. Wong, B. Nagarajan, J. K. Buatis, L. M. Ortega, N. Nandakumar, A. Khanna, V. Shanmugam, S. Dutttagupta, *Sol. Energy Mater. Sol. Cells* **2019**, 192, 109.
- [12] S. Kluska, T. Hatt, B. Grübel, G. Cimiotti, C. Schmiga, V. Arya, B. Steinhauser, F. Feldmann, J. Bartsch, B. S. Goraya, S. Nold, A. A. Brand, J. Nekarda, M. Glatthaar, W. S. Glunz, *Photovolt. Int.* **2020**, 98, 98.
- [13] B. Kafle, B. S. Goraya, S. Mack, F. Feldmann, S. Nold, J. Rentsch, *Sol. Energy Mater. Sol. Cells* **2021**, 227, 111100.
- [14] F. Feldmann, M. Nicolai, R. Müller, C. Reichel, M. Hermle, *Energy Proc.* **2017**, 124, 31.
- [15] D. Chen, Y. Chen, Z. Wang, J. Gong, C. Liu, Y. Zou, Y. He, Y. Wang, L. Yuan, W. Lin, R. Xia, L. Yin, X. Zhang, G. Xu, Y. Yang, H. Shen, Z. Feng, P. P. Altermatt, P. J. Verlinden, *Sol. Energy Mater. Sol. Cells* **2020**, 206, 110258.
- [16] V. Arya, B. Steinhauser, B. Gruebel, C. Schmiga, N. Bay, D. Brunner, M. Passig, A. A. Brand, S. Kluska, J. Nekarda, *Phys. Status Solidi A.* **2020**, 217, 2000474.
- [17] K. Ramspeck, S. Schenk, D. Duphorn, A. Metz, M. Meixner, *Energy Proc.* **2014**, 55, 133.
- [18] C.-S. Jiang, H. R. Moutinho, S. Johnston, Y. Yan, M. M. Al-Jassim, J. Gorman, A. Blosse, *35th IEEE Photovoltaic Specialists Conference*, IEEE, Piscataway, NJ **2010**, pp. 1721–1726.
- [19] I. Geisemeyer, F. Fertig, W. Warta, S. Rein, M. C. Schubert, *Sol. Energy Mater. Sol. Cells* **2014**, 120, 259.
- [20] F. Edelman, A. Chack, R. Weil, R. Beserman, Y. Khait, P. Werner, B. Rech, T. Roschek, R. Carius, H. Wagner, W. Beyer, *Sol. Energy Mater. Sol. Cells* **2003**, 77, 125.
- [21] B. Fischer, *Doctoral Thesis*, Universität Konstanz, **2003**.